Int J Fract (2010) 165:77–92
DOI 10.1007/s10704-010-9506-5

ORIGINAL PAPER

The evolution of a transverse intra-ply crack coupled to delamination cracks

Z. Q. Zhou · X. J. Fang · B. N. Cox · Q. D. Yang

Received: 6 January 2010 / Accepted: 29 April 2010 / Published online: 29 May 2010

Abstract In this paper nonlinear cohesive fracture models with cohesive parameters and laminar elasticity typical of polymer composites are used to study the initiation and propagation of a transverse intra-ply crack that is coupled to possible delaminations at the ply interfaces in a [0/90/0°] laminate. The evolution of the transverse crack is found to be more complex than previously described, involving initial growth, growth along the ply in a tunneling mode, and expansion across the thickness of the ply in a plane strain mode. For the coupled crack system, two failure modes are distinguished: (1) complete tunneling propagation of the transverse crack before any delamination occurs, followed by delamination initiation and propagation; and (2) simultaneous propagation of the transverse and delaminations cracks. The former process is always stable, is favored by large values of the mode II to mode I toughness ratio and low values of the cohesive strength, and is predicted to be the prevalent failure sequence for polymer composites. The latter process is often unstable, because it tends to occur when the cohesive strength is so high that the stress for initiating the transverse crack exceeds the stress required for its tunneling propagation. The nonlinear fracture models provide a unified description of the entire process of initiation and crack propagation. If the delamination cracks are modeled by linear elastic fracture mechanics, substantially inaccurate predictions result for the onset of delamination cracking and for the tunneling crack initiation from a pre-existing flaw.

Keywords Cohesive modeling · Transverse cracks · Delamination · Polymer-matrix composites · Nonlinear fracture

Z. Q. Zhou · X. J. Fang · Q. D. Yang (✉)
Department of Mechanical and Aerospace Engineering, University of Miami, Coral Gables, FL 33124, USA
e-mail: qdyang@miami.edu

B. N. Cox
Teledyne Scientific Company, Thousand Oaks, CA 91360, USA

1 Introduction

Predicting the failure of polymer matrix composites (PMCs) is complicated by their heterogeneous nature, which gives rise to multiple cracks of different types, interacting strongly as they evolve towards failure. Because of the difficulty of prediction, most composite design and certification is based on empirical approaches, with little use of simulations beyond the elastic regime (Cox and Yang 2006). To allow more rational design, and thus to unlock the full potential of composites, theory must meet the challenge of predicting the coupled evolution of multiple crack types. This paper addresses one principal coupled crack system, consisting of a transverse crack within a single ply and associated delamination cracks between that ply and its neighbors. The details of the initiation of the crack system in a pristine material and its evolution into a

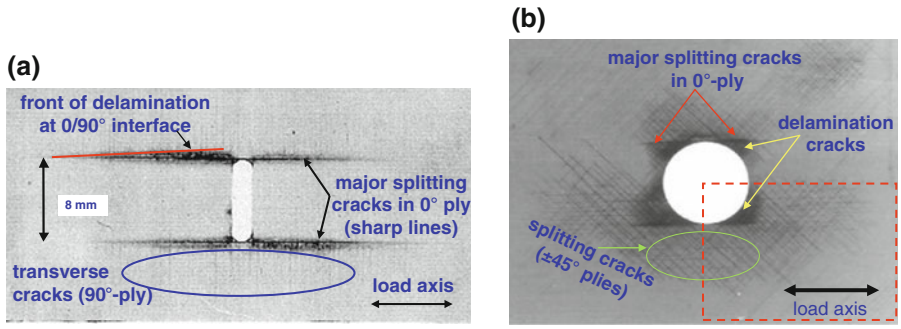

Fig. 1 Images of X-ray radiography showing the coupled damages in (**a**) a $[0/90]_s$ orthotropic laminate with a center slit in tension (Spearing and Beaumont 1992), and (**b**) a $[0/+45/-45/90]_s$ quasi-isotropic laminate with a center hole in tension (Case and Reifsnider 1999)

system of mature cracks are analyzed using nonlinear fracture theory.

The chosen study problem represents much of the main damage observed in tensile tests (Fig. 1). In an orthogonal PMC laminate loaded in tension, dominant splitting cracks appear as sharply defined horizontal lines while wedge-shaped delaminations between the plies appear as areas of shadow around the splitting cracks; and myriad transverse cracks appear in the fiber direction in the transverse plies (Fig. 1a). In a laminate that also contains ±45° fiber plies and a circular hole instead of a slit, substantial differences arise in the splitting crack length and the shape of delaminated areas (Fig. 1b). In both images, the boundaries of the delaminations are correlated with the locations of transverse intra-ply cracks; thus coupled damage evolution dictates the macroscopic composite behavior.

Interlaminar delamination has been extensively studied using methods based on linear elastic fracture mechanics (LEFM), such as the virtual crack closure technique [e.g. (Tay 2003)], as well as cohesive zone models (CZMs) (e.g., (Song and Waas 1994; Shahwan and Waas 1997; Thouless and Yang 2001; Camanho et al. 2003; Yang and Cox 2005). Intra-ply damage modes have been considered under the framework of continuum damage mechanics, e.g. (Chang et al. 1991; McCartney 2003; Cox and Yang 2006; Talreja 2006), where meso-scale averaging invoking assumed periodicity is typically used to obtain homogenized constitutive relations. Direct coupling of intra-ply damage modes represented by continuum damage mechanics with cohesive zone models for discrete delamination cracks has also been attempted recently by several research groups (Camanho et al. 2003; Cox and Yang 2006; Van de Meer and Sluys 2008), but with limited success. Several recent studies have revealed that the homogenization process in continuum damage mechanics loses key information on the coupling of multiple damage mechanisms at the macroscopic scale, causing inaccurate prediction of crack paths (Talreja 2006; Van de Meer and Sluys 2008). Moreover, finite element method (FEM) formulations of continuum damage representations are often subject to non-negligible strain/stress locking (Iarve et al. 2005).

A model that is more physically realistic and complete than continuum damage mechanics has been sought recently by attempting discrete representations of all cracks, of all types, so that their mutual nonlinear coupling can be directly accounted for (Camanho et al. 2006; Cox and Yang 2006; Gonzalez and LLorca 2006; Hallett and Wisnom 2006). Such ambitious discrete crack analyses are enabled by two recent developments, namely improved cohesive zone models for bulk and interface crack problems, which provide a unified physical model for crack initiation and propagation; and new FEM formulations that allow cracks to initiate at arbitrary locations and then propagate along paths that need not be specified in advance, without re-meshing. Formulations in the latter class include the extended FEM or X-FEM (Belytschko and Black 1999; Moes and Belytschko 2002) and the Augmented FEM or A-FEM (Hansbo and Hansbo 2004; Mergheim et al. 2005, 2007; Ling et al. 2009).

Achieving success in simulations of discrete damage also requires guidance from detailed experimental and theoretical studies of damage mechanisms. The catalogue of coupled damage mechanisms and the factors that control them must be complete before multiple-damage formulations can achieve high fidelity. One challenge is to understand the sequences of different cracks (or compound damage modes) that can be expected in ply-scale damage and the physical parameters in material constitutive laws that determine which mode will dominate. A second is to understand the origin of the numerical instabilities that often occur in simulations of heterogeneous materials: are the

instabilities due to numerical approximations or do they reflect physically unstable damage propagation, such as the fast or dynamic crack propagation that is often observed in experiments? How to successfully model cracking sequences and potential instabilities in a computationally cost-effective way is of key interest to developing simulations for use as virtual tests (Cox and Yang 2006).

In this paper, a three-dimensional (3D) analysis based on cohesive zone models is used to investigate the direct coupling between a transverse intra-ply crack (transverse crack) and accompanying delamination cracks. This configuration, sometimes referred to as an H-crack system (Dollar and Steif 1991; Lu 1996), has been the subject of many studies using LEFM (Ye et al. 1992; Ho and Suo 1993; Xia and Hutchinson 1994; Lu 1996; Hoiseth and Qu 2003; Suiker and Fleck 2004). The transverse crack has been postulated to begin as a penny-shaped crack at a localized defect, which then propagates to the ply interfaces and extends through the ply as a tunneling crack. If the tunneling crack cannot penetrate into the neighboring plies, it may induce local delamination at the ply interface.[1]

While LEFM can predict certain trends in crack behavior, as demonstrated in these prior studies, it addresses other issues inadequately. First, since LEFM is only meaningful when a crack already exists, a separate failure criterion must be introduced to predict crack initation in pristine material. Second, once initation is predicted, LEFM cannot describe the transition from uncracked material to a crack that is sufficiently long to be accurately modeled by LEFM; a special numerical procedure must be inserted *ad hoc*, with potential mesh dependence in the resulting predictions. Third, being based on a point process, LEFM fails to treat the effects of the nonlinear facture process zone that exists in reality, which are always important when the zone is comparable in size to geometrical features of the specimen or material, or when multiple cracks interact. Thus the complete evolution from transverse crack initiation (from a flaw) to the complete transverse crack, with potential initiation and propagation of associated delaminations, has not been analyzed in a manner that is physically correct in all conditions.

The paper is organized as follows. Section 2 briefly summarizes the LEFM results of the H-crack system during steady-state propagation in the three-ply symmetric orthogonal laminate [0/90/0], because this limiting case provides guidelines for nonlinear fracture analysis. In Section 3, the coupled transverse and delamination crack system is analyzed using a detailed numerical model with embedded 3D cohesive zone elements on the transverse and delamination crack planes. Section 4 discusses the implications of the results and the limitations of popular practical methods of dealing with numerical instabilities. Section 5 summarizes highlights.

2 Steady-state LEFM analysis of the H-crack propagation in [0/90/0] laminates

Consider the coupled transverse and delamination crack system in an orthogonal [0/90/0] laminate, as shown in Fig. 2a. The laminate is subjected to a displacement controlled remote loading. Each ply is

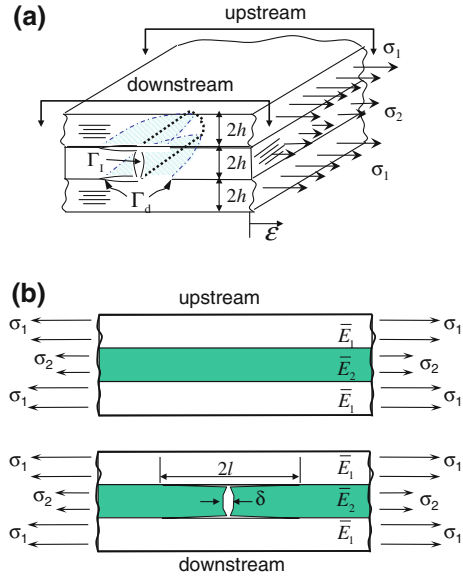

Fig. 2 **a** An illustration of a [0/90/0°] laminate with a steady-state tunneling crack that is accompanied by four delamination cracks (H-crack configuration). The energy that drives the H-crack to advance by a unit depth can be obtained by comparing the strain energy in an upstream slice (*top figure* in **b**) and a downstream slice where the tunneling crack and delamination cracks are fully developed (*bottom figure* in **b**)

[1] An LEFM-based energy criterion for determining whether a tunneling crack penetrates into neighboring plies or is deflected at interface can be found in He and Hutchinson (1989). A more exhaustive criterion based on detailed CZM analysis can be found in Parmigiani and Thouless (2006). The mechanics of crack propagation following penetration has been studied by Cox and Marshall (1996).

transversely isotropic with elastic constants E_1, $E_2(=E_3)$; $\nu_{12}(=\nu_{13})$, ν_{23}, and $G_{12}(=G_{13})$, and thickness $2h$.

For the evolution of the transverse intra-ply crack depicted in Fig. 2, (Ho and Suo 1993) postulated a damage sequence in which, at some initiation stress, a flaw in the transverse ply that is much smaller than the ply thickness will grow first into a penny-shaped crack, which will extend to the ply interfaces, and then propagate through the transverse ply in the fiber direction without penetrating into the neighboring plies. The last phase of growth is the so-called tunneling phase of crack growth, which is characterized by a steady-state configuration, in which the displacement fields far ahead of and far behind the crack tip are invariant (Fig. 2b). The possibility of tunneling-induced delamination was considered by Suiker and Fleck (2004) using LEFM. In the following, relevant simple LEFM results obtained following Suiker and Fleck (2004) are briefly summarized because they provide giudelines for the nonlinear fracture analysis in Sect. 3.

The simple solutions are based on two special problems: (1) the steady-state tunneling phase of the transverse intra-ply crack growth; and (2) the extension in the loading direction of the delamination cracks that may originate at the edges of a tunneling crack (Fig. 2). The tunneling crack can be analyzed by a simple energy analysis, exploiting the invariance of the crack configuration in the far crack wake and the consequent presence there of plane strain conditions (Fig. 2b; Ho and Suo 1993). The delamination propagation is likewise reduced to a plane strain problem if the delaminations grow in the far wake of the tunneling crack; and its analysis is relatively simple if LEFM conditions are assumed to exist at the delamination crack tip. Inferences from these two limiting solutions follow the work of Suiker and Fleck (2004).

2.1 Steady-state tunneling phase of propagation

If the fracture toughness in neighboring plies is sufficiently high, the crack cannot penetrate them, but will propagate only within the 90°-ply along the local fiber direction, achieving the steady-state tunneling crack condition when the crack length increases to several times the ply thickness.

The normalized critical stress for steady-state tunneling is

$$\frac{\sigma_2^{\mathrm{tc}}\sqrt{h}}{\sqrt{\bar{E}_2\Gamma_{\mathrm{II}}}} = \sqrt{\frac{2\Gamma_{\mathrm{I}}/\Gamma_{\mathrm{II}} + 4l/h}{f(\bar{E}_1/\bar{E}_2, l/h)}} \tag{1}$$

where $\bar{E}_1 = E_1/(1-\nu^2)$, $\bar{E}_2 = E_2/(1-\nu^2)$ and $\nu_{12} = \nu_{23} = \nu$ is assumed[2]. Γ_I and Γ_{II} are the mode I and mode II toughness, respectively. In the H-crack problem, the tunneling crack is near mode I and the delamination cracks propagate under near mode II condition (Suiker and Fleck 2004). The dimensionless function $f(\bar{E}_1/\bar{E}_2, l/h)$ can be conveniently obtained through a standard plane-strain finite element analysis of the down-stream problem shown in Fig 2(b) with assumed l/h (Suiker and Fleck 2004). In the limit that $l/h \to \infty$,

$$\frac{\sigma_{2\infty}^{\mathrm{tc}}\sqrt{h}}{\sqrt{\bar{E}_2\Gamma_{\mathrm{II}}}} = \sqrt{\frac{2\bar{E}_1/\bar{E}_2}{\bar{E}_1/\bar{E}_2 + 1/2}} \tag{2}$$

Figure 3 gives calculations of σ_2^{tc} for typical PMCs with $\bar{E}_1/\bar{E}_2 = 12$ and a wide range of values of $\Gamma_{\mathrm{II}}/\Gamma_{\mathrm{I}}$. In this figure, the tunneling initiation stresses in the absence of delamination ($l/h = 0$), $\sigma_{2\_0}^{tc}$, is marked by open circles.

2.2 Delamination propagation in plane strain conditions

From the same plane-strain model (referring to the downstream strip), the energy release rate at a delamination crack tip can also be obtained using the J-integral technique. This energy release rate defines the conditions for delamination propagation from the interface tips of a tunneling crack that has already fully propagated, so that the delamination propagates in plane strain conditions (Fig. 2b). This restrictive assumption about crack geometry will be relaxed in the nonlinear analysis of Sect. 3. The normalized stress for delamination, $\sigma_2^{\mathrm{dc}}\sqrt{h}/\sqrt{\bar{E}_2\Gamma_{\mathrm{II}}}$, as a function of $\bar{E}_1/\bar{E}_2$ and l/h can be dervied as follows,

$$\frac{\sigma_2^{\mathrm{dc}}\sqrt{h}}{\sqrt{\bar{E}_2\Gamma_{\mathrm{II}}}} = \frac{1}{\sqrt{f_d\left(\bar{E}_1/\bar{E}_2, l/h\right)}} \tag{3}$$

[2] Xia et al. (1993) and Xia and Hutchinson (1994) have shown that Poisson's ratios have little influence on steady-state tunneling. For PMCs in which Poisson's ratios for the fibers and matrix are not very different. Therefore one can assume $\nu_{12} = \nu_{23} = \nu$ and focus on the influence of the plane strain Young's moduli.

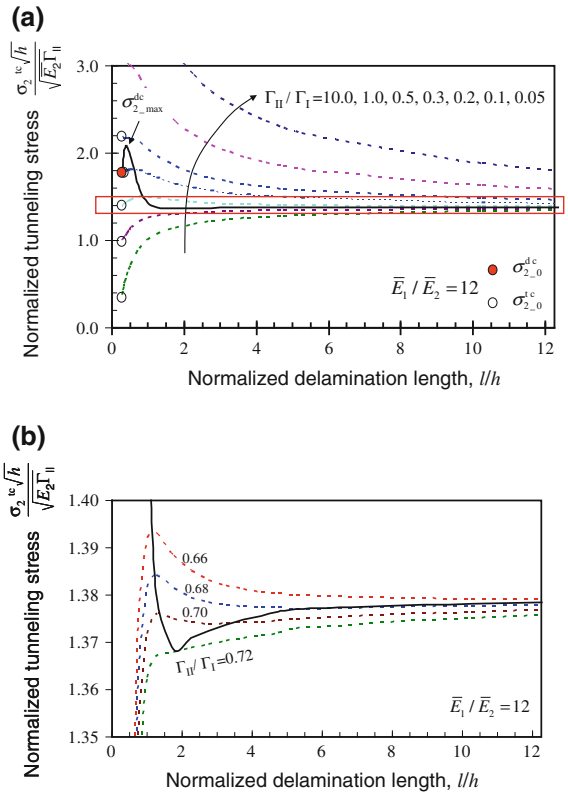

Fig. 3 **a** A normalized tunneling stress as a function of normalized delamination length for a variety of toughness ratios (*dashed lines*). The delamination stress obtained from Eqn. (3) for a plane-strain delamination propagating from a fully propagated tunneling crack is also plotted (*solid curve*). **b** Magnified view of the boxed region in (**a**) showing delamination stress increases as $l/h > 2$, resulting stable delamination growth

where $f_d\left(\bar{E}_1/\bar{E}_2, l/h\right)$ is a dimensionless function that depends on $\bar{E}_1/\bar{E}_2$ and l/h. Suiker and Fleck (2004) proved that $f_d\left(\bar{E}_1/\bar{E}_2, l/h\right) = \partial f\left(\bar{E}_1/\bar{E}_2, l/h\right)/\partial(l/h)$. It can be further proved that as $l/h \to \infty$, the delamination propagation stress, $\sigma^{dc}_{2\_\infty}\sqrt{h}/\sqrt{\bar{E}_2\Gamma_{II}}$, approaches the same limit as the tunneling stress, $\sigma^{tc}_{2\_\infty}\sqrt{h}/\sqrt{\bar{E}_2\Gamma_{II}}$, given in Eq. (2). The computed normalized delamination stress as a function of normalized delamination length for $\bar{E}_1/\bar{E}_2 = 12$ is superimposed on Fig. 3 with delamination initiation stress, $\sigma^{dc}_{2\_0}$, marked as a filled dot. The maximum delamination stress ($\sigma^{dc}_{2\_max}$) is also marked by an arrow.

It is seen that delamination crack propagation is unstable at small crack lengths ($0.2 < l/h < 1$), because the delamination stress, σ^{dc}_2, decreases sharply with the delamination crack length. At steady-state ($l/h > 2$), however, delamination is stable. Further, we found with new calculations that σ^{dc}_2 becomes fairly insensitive to the modulus ratio when $\bar{E}_1/\bar{E}_2 > 5$.

2.3 Inferred failure sequence for coupled tunneling and delamination cracks

Trends in the expected damage sequence can be predicted by comparing the steady-state tunneling stress to the plane-strain delamination stress. Three regimes of behavior are inferred.

(i) *Large delamination toughness*. If Γ_{II}/Γ_I is sufficiently large ($\Gamma_{II}/\Gamma_I > 0.72$), the tunneling stress, $\sigma^{tc}_{2\_0}$, for zero length delamination ($l/h = 0$) is less than the stress for delamination propagation at zero delamination length ($\sigma^{dc}_{2\_0}$ in Fig. 3a). Therefore steady state tunneling will be achieved without delamination. If the load is then increased, delamination will occur at the stress $\sigma^{dc}_{2\_0}$, where delamination will begin. Stable delamination propagation will ensue as the stress is raised to $\sigma^{dc}_{2\_max}$ in Fig. 3a, where the delamination length is approximately $l/h = 0.2$. When $0.2 < l/h < 2.0$, delamination is unstable. However, as $l/h > 2.0$ it will regain stability for all $l/h \to \infty$.

(ii) *Intermediate delamination toughness*. If Γ_{II}/Γ_I takes an intermediate value ($0.21 < \Gamma_d/\Gamma_I < 0.72$), then $\sigma^{tc}_{2\_0}$ exceeds $\sigma^{dc}_{2\_0}$, but is less than $\sigma^{dc}_{2\_max}$. Therefore, some delamination will accompany the propagation of the tunneling crack, with a delamination length fixed by the condition that $\sigma^{dc}_2(l) = \sigma^{tc}_2$. When tunneling is complete, further stress increase up to $\sigma^{dc}_{2\_max}$ will cause stable delamination propagation when $l/h < 0.2$. When $0.2 < l/h < 2.0$, delamination is unstable. However, as $l/h > 2.0$ it will regain stability for all $l/h \to \infty$.

Small delamination toughness. If Γ_{II}/Γ_I is sufficiently small ($\Gamma_{II}/\Gamma_I < 0.21$), then $\sigma^{tc}_{2\_0}$ exceeds $\sigma^{dc}_{2\_max}$. Steady state tunneling crack propagation will be accompanied by immediate delamination propagation, which will be unstable to $l/h \to \infty$.

The above limiting-case solutions cannot describe coupled crack evolution in which plane conditions do not exist, and are therefore not applicable to the first

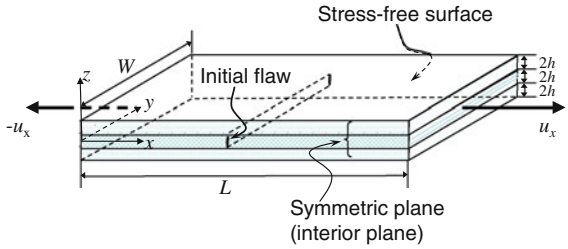

Fig. 4 The [0/90/0] laminate analyzed using nonlinear fracture models. Only half of the model ($Z < 0$) was modeled due to symmetry. Cohesive elements were planted along the interface and in the middle of the 90°-ply

stages of initiation; nor do they account for the influence of material nonlinearity, which is expected to be significant for a polymer composite, because the nonlinear fracture process zone is comparable to or larger than the ply thickness. Nevertheless, the identified trends form a basis for interpreting the detailed nonlinear fracture analysis presented in the next section.

3 Nonlinear fracture analysis

3.1 Numerical model with embedded cohesive elements

This section addresses the questions of initiation and early coupled growth of transverse intra-ply (transverse) and delamination cracks using nonlinear fracture analysis, based on cohesive zone modeling.

The 3D problem of Fig. 1(a) was studied numerically using the model shown in Fig. 4. Displacement controlled loading was prescribed at both ends, $x = 0$ and $x = L$. Due to symmetry about the mid-laminate plane $z = 0$, only one half of the specimen ($z \leq 0$) was modeled. Symmetry also exists about the mid-span plane, $x = L/2$, but this was not exploited because it is inconvenient to handle cohesive elements on the plane $x = L/2$ if that plane hosts a crack and is also a model-bounding plane. Symmetric boundary conditions ($u_y(x, 0, z) = 0$; $\partial u_y(x, 0, z)/\partial y = 0$) were prescribed on the surface y = 0, while the surfaces $y =$ W and $z = -3h$ were set to be stress-free.

Cohesive zone elements were placed in the 90° ply in the mid-span plane ($x = L/2, -h \leq z \leq 0$) as illustrated in Fig. 4. The initial stiffness of the cohesive law for these cohesive elements was made sufficiently large that the cohesive surface does not behave like a pre-existing crack; until damage occurs, the material deformation is homogeneous in the neighborhood of the potential crack plane. To facilitate transverse intra-ply crack initiation, the cohesive element at the mid-point of the specimen ($x = L/2$; $z = 0$; $y = 0$), which lies in the potential transverse crack plane, was assigned a smaller strength and toughness. Initiation is then expected either at this mid-specimen location or at the stress-free specimen edge.

The interface between the 0 and 90° plies ($z = -h$) were also modeled by cohesive elements.

3.2 Cohesive law, elastic, and geometrical parameters

The 3D cohesive zone model used here is similar to that used by Yang and Cox (2005). Independent cohesive traction-separation laws are included for the opening mode (mode I) and shear modes (modes II and III), so that the toughness (total area underneath the cohesive law) and cohesive strength can vary between the three modes. As appropriate for polymer composites, the toughness and strength are assigned to be the same for modes II and III, but different for mode I (Borg et al. 2004; Camanho et al. 2003; Yang and Cox 2005). Equality for modes II and III can be anticipated from considerations of mechanisms: the material in the crack tip process zone is likely to be insensitive to the direction of any shear deformation it undergoes. For example, fibrils drawn out in a craze zone between the fracture surfaces in mode I are locally isotropic in the fracture plane. They will shear equally in either direction within the crack plane under subsequent mode II or mode III loading.

The cohesive zone model accommodates separation of the total energy absorbed during fracture, G, into opening and shear components, G_{I}, G_{II} and G_{III}:

$$G = G_{\mathrm{I}} + G_{\mathrm{II}} + G_{\mathrm{III}} \tag{4}$$

The separate components can be calculated by integration of the mode I, II and III traction-separation curves (Fig. 5):

$$G_{\mathrm{I}}(\delta_n) = \int_0^{\delta_n} \sigma(\delta_n')\, d\delta_n'; \tag{5a}$$

$$G_{\mathrm{II}}(\delta_{tx}) = \int_0^{\delta_t} \tau_x(\delta_{tx}')\, d\delta_{tx}' \tag{5b}$$

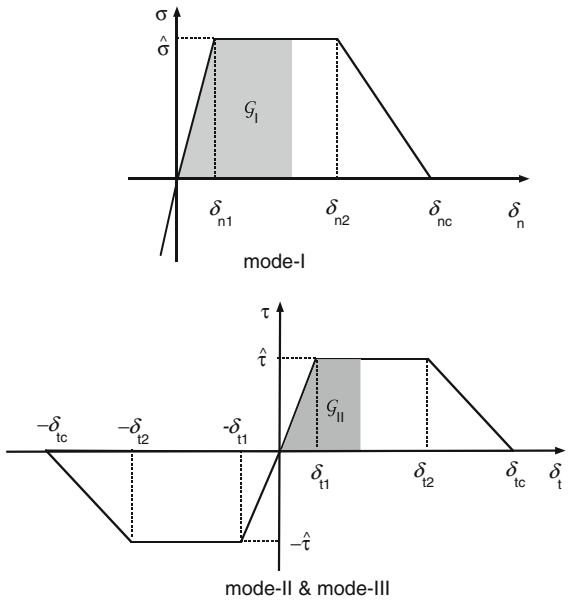

Fig. 5 A mode-dependent cohesive zone model proposed by Yang and Thouless (2001)

$$G_{\mathrm{III}}\left(\delta_{ty}\right) = \int_0^{\delta_{ty}} \tau_y(\delta'_{ty}) d\delta'_{ty} \tag{5c}$$

where δ_n, δ_{tx}, and δ_{ty} are the mode I, II, and III displacement jumps across the interface and σ, τ_x, and τ_y are the corresponding mode I, II, and III cohesive tractions, respectively. The energy release rate components are not independent parameters; they evolve together as a natural result of the interplay between the deformation of the plies and the physics embedded in the traction-separation laws. A failure criterion is required to specify conditions for complete separation to traction-free conditions (failure) in the cohesive zone. The criterion used here is a simple one (Wang and Suo 1990; Hutchinson and Suo 1992):

$$D = G_{\mathrm{I}}/G_{\mathrm{I}}\left(\delta_{\mathrm{nc}}\right) + G_{\mathrm{II}}/G_{\mathrm{II}}\left(\delta_{\mathrm{txc}}\right) + G_{\mathrm{III}}/G_{\mathrm{III}}\left(\delta_{\mathrm{tyc}}\right) = 1 \tag{6}$$

where D is a damage measure ranging from 0 (undamaged) to 1 (fully debonded). When $D = 1$, all tractions are set to zero, even though individual displacement components will not generally have reached the limiting values, δ_{nc} or δ_{tc}, shown in Fig. 5.

In the problem shown in Fig. 4, the tunneling crack is mode I while the delamination cracks are generally close to mode II. Nevertheless, a unified mixed-mode cohesive law was assigned to the cohesive elements, because it has been repeatedly proven that the cohesive model presented here is able to capture accurately the mode mixedness according to local stress conditions (Yang et al. 2010; Parmigiani and Thouless 2006)

Each of the traction-separation laws is piece-wise linear with four selectable parameters: the cohesive strength, the fracture toughness, and two intermediate displacements that control the shape of the law (slopes of segments). Many previous studies have shown that the cohesive strength and toughness are the most important parameters for cohesive fracture analysis, while the detailed shape of the traction separation law is of secondary importance (Tvergaard and Hutchinson 1993; Yang and Thouless 2001). In this study, the mode-I cohesive law has toughness, $G_{\mathrm{I}}\left(\delta_{\mathrm{nc}}\right) = \Gamma_{\mathrm{I}}$ and cohesive strength $\hat{\sigma}$. The mode-II cohesive law (identical with mode III) has toughness $G_{\mathrm{II}}\left(\delta_{\mathrm{tc}}\right) = \Gamma_{\mathrm{II}}$ and cohesive strength, $\hat{\tau}$. Thus the complete set of model parameters reduces to $\chi_1 = \bar{E}_1/\bar{E}_2$, $\chi_2 = \hat{\sigma}/\bar{E}_2$, $\chi_3 = \Gamma_{\mathrm{II}}/\Gamma_{\mathrm{I}}$, $\chi_4 = \Gamma_{\mathrm{I}}/\bar{E}_2 h$, and $\chi_5 = \hat{\sigma}/\hat{\tau}$.

For a crack in an infinite body with modulus E governed by a cohesive law with energy Γ and strength σ, the length of the cohesive zone is a material property, given approximately by $l_{\mathrm{ch}} = E\Gamma/\sigma^2$ (Cottrell 1963; Hillerborg et al. 1976; Rice 1980). For the transverse intra-ply crack, the associations $\Gamma \to \Gamma_I$, $E \to \bar{E}_2$, and $\sigma \to \hat{\sigma}$ are most reasonable,[3] giving

$$\frac{l_{\mathrm{ch}}^I}{h} = \left(\frac{\Gamma_{\mathrm{I}}}{\bar{E}_2 h}\right)/\left(\frac{\hat{\sigma}}{\bar{E}_2}\right)^2 = \frac{\chi_4}{\chi_2^2} \tag{7a}$$

i.e., the proportion of the cohesive zone length to the ply thickness is governed by the parameters χ_2 and χ_4. For a mode II delamination crack in a laminate with relatively small sublaminate thickness t, the length of the cohesive zone is no longer a simple material property, but is a structure-material parameter given approximately by $l_{\mathrm{ch}} = (E\Gamma/\sigma^2 \cdot t)^{1/2}$ (Massabò and Cox 1999). For the interply delamination cracks, the associations $\Gamma \to \Gamma_{\mathrm{II}}$, $E \to \bar{E}_2$, $\sigma \to \hat{\tau}$, and $t \to h$ lead to

$$\frac{l_{\mathrm{ch}}^{\mathrm{II}}}{h} = \left(\frac{\Gamma_{\mathrm{I}}}{\bar{E}_2 h}\frac{\Gamma_{\mathrm{II}}}{\Gamma_{\mathrm{I}}}\right)^{1/2}/\left(\frac{\hat{\sigma}}{\bar{E}_2}\right) = \frac{\sqrt{\chi_4\chi_3}}{\chi_2} \tag{7b}$$

[3] For both the transverse intra-ply crack and the delamination crack, most of the strain release associated with the crack advance consists of lowering of the component ε_x of strain in the transverse ply, where x is the load axis. Thus the germane modulus for both cracks is E_2, not E_1.

i.e., the proportion of the cohesive zone length in the delamination crack to the ply thickness is governed by the parameters χ_2, χ_3, and χ_4.

The influence of specimen and material dimensions on the nonlinear fracture problem is characterized by Eq. (7): the particular choice of ply thickness is not important, but its proportion to the lengths l_{ch}^{I} and l_{ch}^{II} is vital. Other specimen dimensions (width, length, etc.) are unimportant, as long as they greatly exceed l_{ch}^{I} and l_{ch}^{II}. Therefore, the role of length scales in the problem can be surveyed by varying just χ_2 and χ_3 while holding χ_4 fixed. In the following studies, χ_4 was assigned the fixed value $\chi_4 = \Gamma_I/\bar{E}_2 h = 4.6 \times 10^{-4}$, a typical value for a polymer composite.

In this study the modulus ratio $\chi_1 = \bar{E}_1/\bar{E}_2 = 12$ was not varied and the ratio $\chi_5 = \hat{\sigma}/\hat{\tau}$ was fixed at the value $\chi_5 = 1$. For matrix-mediated failure mechanisms, strong variation in the ratio of tensile and shear strengths is not expected; a survey of opening and shear cohesive strengths used in literature shows $\hat{\sigma}/\hat{\tau}$ values are never far away from unity.

With the understanding that the ply thickness $2h$ enters only through the ratios l_{ch}^{I}/h and l_{ch}^{II}/h and that the specimen length and width need only be large compared to l_{ch}^{I} and l_{ch}^{II}, the absolute model dimensions $L = W = 10\,\text{mm}$ and $2h = 0.2\,\text{mm}$ were chosen for the study problem. With the similar understanding that Young's moduli enter only via the parameters χ_1, χ_2, and χ_4, while Poisson's ratios and the shear moduli have only weak influence, the particular transversely isotropic elastic constants chosen for each ply were listed in Table 1.

3.3 Simulations of damage evolution

The cohesive model enables a unified description of the entire process of coupled damage evolution, including transverse intra-ply (transverse) crack initiation at either the embedded flaw or the free edge, the linking of these two initiation events, the initiation of associated delaminations, and the maturation of the transverse crack as the delaminations grow longer until the transverse crack is traction-free.

The simulations reveal that the transverse crack does indeed initiate from the introduced flaw as a penny-shaped crack before it reaches the interface. However, the simulated process of how this penny-shaped crack turns into a mature transverse crack is different from what was postulated in literature (e.g., Ho and Suo 1993); in particular, the stress-free edge and the nonlinearity of the fracture process both have a significant influence on the process. The same cohesive law is used in modeling both the transverse and interface cracks. Since the transverse crack is predominantly mode I and an interface crack is predominantly mode II, using the same multi-mode law for both presents no unreasonable restriction on generality. In the following, "interface toughness" refers to the mode-II toughness, Γ_{II}, of the cohesive law, while the mode-I toughness, Γ_I, characterizes the transverse crack. The "cohesive strength" refers to the critical stress for activating a nonlinear fracture process zone, i.e., crack initiation in pristine material.

In the following study of the effects of changing the relative interface and transverse crack toughness, the mode I and mode II toughness values were varied by changing the critical displacement, δ_{tc}, in the mode II law, while the mode I and mode II cohesive strength parameters, $\hat{\sigma}$ and $\hat{\tau}$, were kept equal and constant.

Two failure modes are distinguished for the coupled crack system: (1) complete tunneling propagation of the transverse crack before any delamination occurs, followed by delamination initiation and propagation, which occurs when interface toughness is relatively large compared to mode I toughness or cohesive strength is low; and (2) simultaneous propagation of the transverse and delaminations cracks, which occurs when interface toughness is much smaller than mode I toughness, or cohesive strength is very high. Figure 6 gives sequential snap shots of the coupled nonlinear evolution for each case. In this figure, the domain $x > L/2$ in the 90°-ply has been removed to facilitate viewing of the delamination crack.

Table 1 Transversely isotropic elastic constants used for each ply in this study

Longitudinal modulus (E_1)	Transverse modulus (E_2)	Out-of-plane shear modulus (G_{12})	ν_{12}	ν_{23}
(GPa)	(GPa)	(GPa)	–	–
165.4	12.95	6.96	0.21	0.30

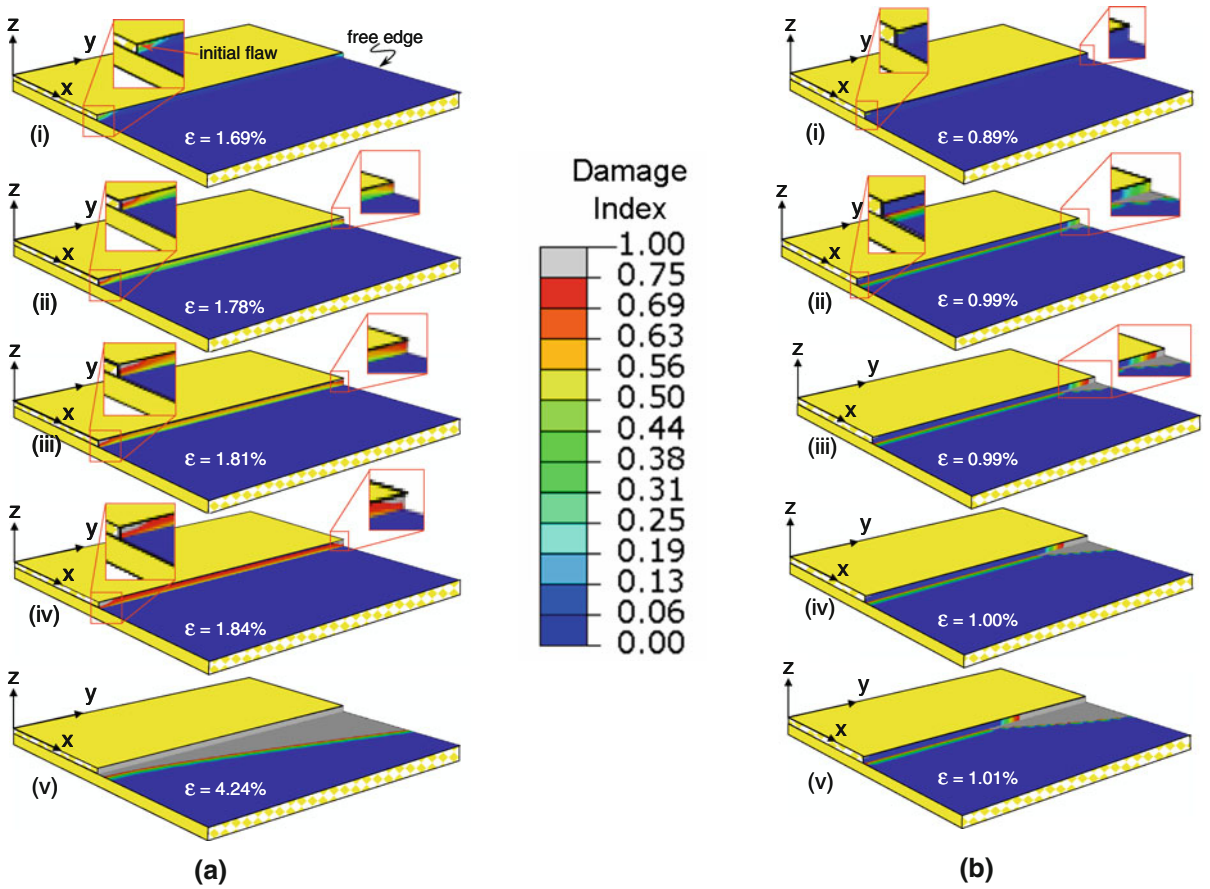

Fig. 6 Sequential snap-shots showing two possible sequences of damage evolution along the cracking planes. The nearer half of the 90°-ply has been removed to facilitate the view of delamination and tunneling crack propagation. The mode II toughness has been varied by varying the critical mode II cohesive displacement. The nominal strains corresponding to each snap shots are labeled on each graph. (**a**) Tunneling without delamination ($\Gamma_I/\Gamma_{II} = 2.0$; $\hat{\sigma}/E_2 = 0.004$). (**b**) Tunneling with delamination ($\Gamma_{II}/\Gamma_I = 0.1$; $\hat{\sigma}/E_2 = 0.008$)

(i) Large interface toughness. If the interface toughness is sufficiently large compared to that of the transverse crack ($\chi_3 = \Gamma_{II}/\Gamma_I > 0.2$), the damage sequence contains the following distinct phases.

- The penny-shaped crack spreads from the interior defect towards the transverse ply interfaces (Fig. 6a-(i)).
- When a/h reaches a value of about 0.7 (with $2a$ the diameter of the penny crack and $2h$ the ply thickness), a mode I cohesive crack starts to develop from the specimen edge (Fig. 6a(ii)).
- The penny crack and the edge crack propagate towards one another in a tunneling mode, forming a single transverse crack (Fig. 6a-(iii)). During this tunneling phase, the crack displacement is restricted by the constraint of the neighboring 0° plies and remains less than the critical displacement, δ_{nc}, over most of the tunneling system (Fig. 6a-(iv)).
- Upon small further load increments (3–5% increase of σ_2), the transverse crack spreads through the thickness of the ply under approximately plane strain conditions, with increasing mode I displacements (i.e., increasing degrees of cohesive damage) as it approaches the ply interfaces (Fig. 6a-(iv)). This stage of evolution precedes any delamination damage on the interface.
- At some point during the opening of the tunneling crack with increasing load, delamination damage occurs at the interface (the transition region from

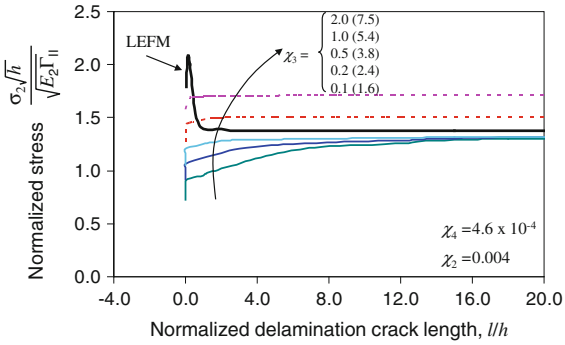

Fig. 7 Normalized stresses versus delamination length predicted by nonlinear fracture analysis, for five different toughness ratios, leading to five different normalized cohesive zone lengths, as indicated by numbers in parentheses following the χ_3 values. The lowest point of each curve corresponds to the stress level at which the tunneling process is just completed. The two *dashed curves* were obtained using viscous damping method, but exhibit incorrect delamination stresses—see text

blue to silver), first at the free edge (Fig. 6a-(iv)) and then propagating quickly into the specimen interior. The delamination crack then propagates in the direction of the load axis until nearly complete delamination occurs (Fig. 6a-(v)). As the delamination develops, the opening of the transverse crack increases, until the transverse crack is completely stress-free.

This sequence of coupled damage progression will be termed "tunneling without delamination", since delamination cracks do not develop before the tunneling process has run the length of the ply.

Mechanics of delamination that follows tunneling. Predicted curves of delamination stress ($\sigma_2^{dc}\sqrt{h/\bar{E}_2\Gamma_{II}}$) vs. delamination crack length (l/h) for five different toughness ratios ($\chi_3 = 0.1, 0.2, 0.5, 1.0, 2.0$) and $\chi_2 = 0.004$ are plotted in Fig. 7. For all five cases, delamination occurred after the transverse crack tunneled across the entire specimen (tunneling-without-delamination mode). Therefore delamination occurs in nearly plane-strain conditions, apart from minor variations near the specimen edges. Each curve starts with the stress level at which the tunneling process has just concluded. From this point, further increase of the stress is needed to initiate delamination. Delamination crack growth after the delamination initiation stress is reached is initially stable: the delamination stress increases slightly with increasing l/h, where conditions are closest to plane strain. As l/l_{ch}^{II} becomes larger than ~2, all curves converge to a steady-state solution that is in good agreement with LEFM. The difference between the tunneling stress and the steady-state delamination stress decreases with decreasing toughness ratio.

(ii) Small interface toughness. If χ_3 is sufficiently small (<0.2), the transverse crack initiation process from the induced flaw site remains similar (Fig. 6b-(i)) to that observed in the tunneling-without-delamination mode. However, for the particular strength assigned to the embedded flaw, the transverse crack initiates from the specimen edge (Fig. 6b-(ii)) instead of from the initial flaw site. The reason for this is found in the following trends:

- the energy release rate for a small, incipient transverse ply crack is increased substantially if the adjacent interface fails;
- interface failure tends to happen more readily at the free edge, where both mode II and mode III sliding components can contribute to strain relaxation (observe the more rapid advance of the delamination near the free edge than near the center of the specimen in Fig. 6a, for example);
- as the interface toughness becomes lower, the extent of the interface failure that accompanies incipient transverse crack development at the free edge increases and therefore the gain in the energy release rate for the transverse crack at the free edge relative to the incipient transverse crack at the embedded defect increases.

Through the interplay of these trends, a transition in failure mode occurs at a sufficiently low, critical value of the mode II toughness: failure occurs by the tunneling propagation of a transverse crack from the specimen edge that is accompanied by simultaneous, extensive delamination (Fig. 6b). This mode will be called "tunneling with delamination."

The delamination process in the tunneling-with-delamination mode is characterized by an approximately triangular delamination zone (Fig. 6b-(iii–v)), rimmed by a significant band of cohesive damage (incompletely failed material), which propagates ahead of the traction-free tunneling crack front. The delamination propagates along the tunneling direction and the load axis simultaneously, and appears to be unstable.

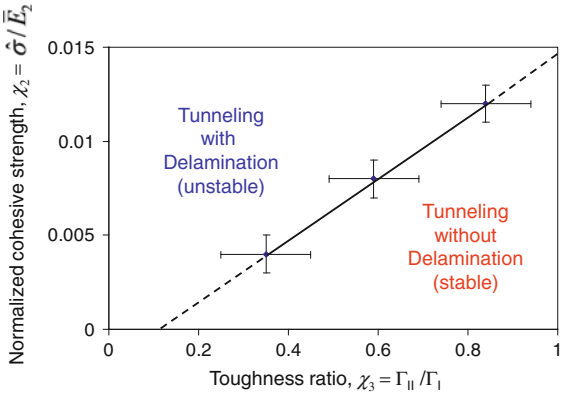

Fig. 8 Numerically determined boundary between the tunneling-without-delamination and tunneling-with-delamination modes on $\hat{\sigma}/\bar{E}_2 - \Gamma_{II}/\Gamma_I$ plane

3.3.1 Failure map in strength-toughness space

The boundary between the tunneling-without-delamination and tunneling-with-delamination modes was determined as a function of the mode II to mode I toughness ratio, $\chi_3 = \Gamma_{II}/\Gamma_I$, and the cohesive strength normalized against the material stifffness, $\chi_2 = \hat{\sigma}/\bar{E}_2$. When the cohesive strength was varied, the ratio of the strengths in modes I and II, $\chi_5 = \hat{\sigma}/\hat{\tau}$ was kept fixed at the value $\chi_5 = 1$. The numerically determined boundary between the stable tunneling-without-delamination and the unstable tunneling-with-delamination modes is shown in Fig. 8 for feasible normalized strength values. The error bars shown reflect the difficulty in distinguishing stable and unstable calculations near the boundary. The boundary is approximately a linear function between χ_2 and χ_3.

The modes of failure in the two failure domains were always qualitatively similar to the examples shown in Fig. 6. In particular, in the tunneling-with-delamination domain, steady-state tunneling with fixed delamination crack length, which was an assumed crack configuration in the LEFM work reviewed in Sect. 2, does not occur within the parameter range investigated ($\Gamma_{II}/\Gamma_I = 0.1 - 2.0$ and $\hat{\sigma}/\bar{E}_2 = 0.004 - 0.008$).

The failure map shows that the tunneling-with-delamination mode occurs only for small relative mode II toughness. In polymer composites, the mode II toughness is generally higher than the mode I toughness, due to friction and other phenomena. Therefore, the tunneling-with-delamination mode will not be commonly observed in polymer composites, unless a mechanism for suppressing transverse cracking is incorporated by materials modification.

3.3.2 Length scale considerations

For the tunneling-without-delamination mode, in which full delamination can be captured by the nonlinear fracture analysis, the predicted curves are significantly different from the LEFM prediction at small delamination crack length ($l/l_{ch}^{II} < 2$). LEFM predicts a diverging critical stress for vanishing crack length, whereas the cohesive model introduces initial damage at a local stress that never exceeds $\hat{\sigma}$. The delamination crack lengths for which LEFM breaks down are comparable to or less than the characteristic cohesive zone length, l_{ch}^{II}, of Eq. (7).

From Eq. (7), l_{ch}^{II} increases with the delamination toughness. Within typical values for $\chi_4 = 4.6 \times 10^{-4}$ and $\chi_2 \cong 0.004$, l_{ch}^{II}/h ranges approximately from 2 to 8 as $\chi_3$increases from 0.1 to 2. Therefore the cohesive zone size is on the order of a few times the ply thickness, which is confirmed by Fig. 6 (the width of the transition region from undamaged to traction-free material; blue to silver).

The presence of the delamination cohesive zone tends to stabilize crack propagation, especially at small delamination length, $l/l_{ch}^{II} < 2$. If χ_3 is relatively large ($\chi_3 > 1$), the development of the cohesive zone requires a considerable stress increase as *l/h* increases (Fig. 7). As χ_3 gets smaller, a smaller cohesive zone is developed and the stabilizing effect diminishes; the difference between the tunneling and delamination stresses is much smaller and steady-state delamination almost immediately follows delamination initiation.

3.3.3 Treatment of instability

When $l/l_{ch}^{II} > 2$, all predicted delamination curves converge (within a numerical error of 5%) to the steady-state solution of LEFM (Fig. 7); under such conditions LEFM is valid. However, when χ_3 becomes smaller than $\sim$ 0.2 and therefore $l/l_{ch}^{II} < 2$ for the parameter values used in Fig. 7, the tunneling stress becomes larger than the steady-state delamination stress and tunneling is accompanied by delamination (tunneling-with-delamination mode). In such cases, numerical instability prevents simulation of the complete tunneling with delamination process, unless some numerical stabilization technique is used. One

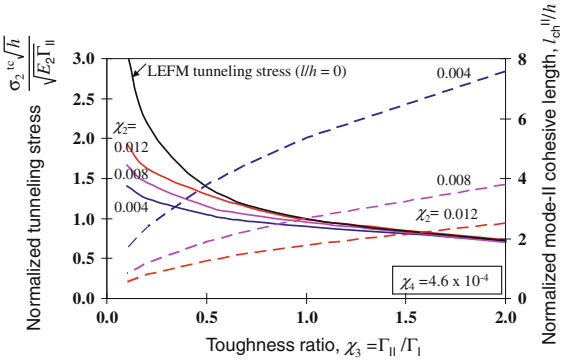

Fig. 9 Predicted tunneling stresses in nonlinear fracture model as functions of toughness ratios for three cohesive strengths (*solid lines*). The predicted curve for LEFM is plotted for comparison

method offered by ABAQUS is a stabilization function, which introduces artificial viscous damping *into the global stiffness matrix*. The two dashed lines in Fig. 7, corresponding to the unstable cases of $\chi_3 = 0.1$ and 0.2, were obtained with the help of this artificial viscous-damping. For these cases, the predicted steady-state propagation stress values are incorrect; they do not satisfy the expected analytical limit. Thus the viscous-damping method has introduced spurious material properties, which harm the fidelity of the calculation.

The arc-length method (RIKS method in ABAQUS) was also tried but without success for this problem. The arc-length method is effective for problems with instabilities induced by geometric nonlinearity (Geers 1999; Zhang and Wang 2009). However, here the instability is mostly caused by localized material nonlinearity. For such a problem, the recently proposed dissipation based arc-length method may be more effective (Verhoosel et al. 2008). However, this was not pursued in this study.

3.3.4 Tunneling stress as a function of toughness ratio

The predicted tunneling stresses are plotted as functions of the toughness ratio for three cohesive strengths in Fig. 9. The tunneling stress for the tunneling-without-delamination mode was defined as the point where the tunneling crack has just traversed the specimen, but not yet spread through the thickness of the transverse ply all the way to the ply interfaces (Fig. 6a-iv). For the tunneling-with-delamination mode, the tunneling stress was defined as the point where the tunneling crack starts to propagate from the specimen edge into the specimen (Fig. 6b-iii). LEFM predicts that the tunneling stress in the absence of delamination ($l/h = 0$) is a function of the toughness ratio only, scaling with $(\Gamma_{II}/\Gamma_I)^{-1/2}$ (see Eq. 1). This is shown in Fig. 9 by the solid line marked "LEFM tunneling stress." The nonlinear fracture model results show that the tunneling stress is also moderately dependent on the cohesive strength, $\chi_2 = \hat{\sigma}/\bar{E}_2$.

The nonlinear fracture predictions have a similar trend to the LEFM result in that $\sigma_2^{tc}\sqrt{h}/\sqrt{\bar{E}_2\Gamma_{II}}$ decreases monotonically with increasing $\chi_3 = \Gamma_{II}/\Gamma_I$. In the limit of large $\chi_3(\chi_3 > 1)$, the nonlinear fracture results are fairly close to the LEFM prediction. In this limit, the strong interface ensures tunneling through to the stress-free edge without delamination and the nonlinear fracture solution should approach the classic steady-state tunneling problem as studied by Ho and Suo (1993). In the opposite limit of small χ_3, however, the $\sigma_2^{tc}\sqrt{h}/\sqrt{\bar{E}_2\Gamma_{II}}$ values predicted by nonlinear fracture are considerably smaller than the LEFM predictions. In this limit, the interface is relatively weak and provides diminishing constraint to tunneling crack propagation in the transverse ply. The singular stress field assumed in LEFM leads to the prediction that $\sigma_2^{tc}\sqrt{h}/\sqrt{\bar{E}_2\Gamma_{II}}$ remains proportional to $\left(\sqrt{\Gamma_{II}/\Gamma_I}\right)^{-1}$. However, the nonlinear fracture model does not support a singular crack stress field and the maximum stress that can be supported in a cohesive zone is limited by the cohesive strength. Hence the predicted $\sigma_2^{tc}\sqrt{h}/\sqrt{\bar{E}_2\Gamma_{II}}$ is smaller than that of LEFM.[4] Increasing the cohesive strength will bring the tunneling stress curve closer to the LEFM result, which is evident in Fig. 9.

3.3.5 Delamination initiation stress

While the LEFM can predict well the tunneling stress in PMCs with relatively large $\Gamma_{II}/\Gamma_I(> 1)$, it is not accurate in capturing the delamination initiation process. The CZM predicted delamination initiation stresses as functions of toughness ratio are plotted in Fig. 10 (solid lines with symbol), together with the steady-state CZM delamination stress (solid line without symbol) and steady-state LEFM result (dashed line

[4] The fact that the remote stress to drive a cohesive crack with finite cohesive strength is typically smaller than the stress to drive a singular LEFM crack has been seen in many studies with various geometries, e,g, Cavalli and Thouless (2001) and Yang, Cox, et al. (2006).

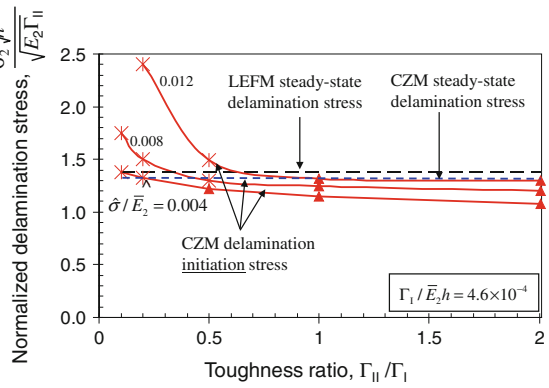

Fig. 10 CZM predicted delamination initiation stresses as functions of toughness ratio for three cohesive strengths (*solid line with symbols*). The CZM predicted steady-state delamination stress and LEFM predicted steady-state delamination stress are also superimposed for comparison. The numerical stability of each case is indicated by the symbol associated with each data point: * means a simulation is unstable and *filled triangle* denotes a stable simulation

without symbol). In this figure, the data points with filled triangular symbols indicate that in these simulations stable tunneling-without-delamination modes were observed; while the data points with symbol * indicate unstable tunneling-with-delamination mode prevailed in the simulations. It appears one can conclude that the unstable tunneling-with-delamination mode occurs whenever the delamination initiation stress is larger than the steady-state delamination stress.

Also, from the normalized plot of Fig. 10, it appears that the normalized delamination initiation stress decreases with the increase of toughness ratio, which is seemingly unphysical. This is caused by the particular choice of normalization of the delamination stress, in which the non-normalized stress is divided by the square root of Γ_{II}. However, if one takes Γ_{II} to be a fixed value and changes the tunneling toughness (Γ_I) to achieve variation of the toughness ratio, the physical meaning of the delamination initiation curves is apparent: reducing Γ_I (i.e., increasing Γ_{II}/Γ_I) results in a reduced delamination initiation stress. Further, the delamination initiation stress shows a mild increase with the cohesive strength. Note that a higher cohesive strength combined with a smaller delamination toughness results in a solution closer to the LEFM result. This aspect is correctly captured by the initiation curves with $\hat{\sigma}/E_2 = 0.008$ and 0.012 at small Γ_{II}/Γ_I.

The steady state delamination stresses (large l/h) for all toughness ratios are all close to the LEFM solution of Eq. (3) (within 5%) and is fairly independent of $\hat{\sigma}/E_2$, which is consistent with the fact that LEFM is accurate when the delamination crack length is sufficiently larger than the cohesive fracture zone size. The LEFM solution of Eq. (3) is accurate for computing the delamination stress in the steady state, i.e., with delamination larger than $l/l_{ch}^{II} > 2$.

4 Discussion

4.1 Implications to failure criterion of transverse matrix cracking

Of the two modes (tunneling-without-delamination & tunneling-with-delamination) observed in the current nonlinear fracture analyses, the tunneling-without-delamination mode is the more frequently reported in experimental studies. For example, in the experimental reports of (Spearing and Beaumont 1992; Hallett and Wisnom 2006), there was little evidence that delamination accompanied the development of transverse cracks, which typically occurred well below the final failure load. Widespread delamination occurred only when final load was approached. This experimental observation can be readily explained by the current analysis result: for typical PMCs the mode-I toughness, which is responsible for the tunneling cracks in transverse plies, is typically smaller than the near mode-II delamination toughness (Turon et al. 2005; Hallett and Wisnom 2006), i.e., Γ_{II}/Γ_I remains larger than 1. Under such conditions, the delamination initiation stress is typically larger than the tunneling stress (Fig. 7). Hence there will be no delamination accompanying the steady-state tunneling process. However, under increased loading, the delamination will eventually occur[5].

More over, since in the limit of $\Gamma_{II}/\Gamma_I > 1$ the normalized tunneling stress, $\sigma_2^{tc}\sqrt{h}/\sqrt{\bar{E}_2\Gamma_{II}}$, is proportional to $\left(\sqrt{\Gamma_{II}/\Gamma_I}\right)^{-1}$ (Fig. 9), it follows from Eq. (1) that the non-normalized tunneling stress is independent of the interface delamination toughness, Γ_{II}, i.e,

$$\sigma_2^{tc} = \sqrt{\frac{2\bar{E}_2\Gamma_I}{hf(\bar{E}_1/\bar{E}_2)}} \tag{8}$$

[5] After tunneling through, another failure mechanism that may compete with local delamination is multiple transverse cracking, but this is beyond the focus of this paper.

The non-dimensional function $f(\bar{E}_1/\bar{E}_2)$ has been calculated by Ho and Suo (1993) and is found to be $f \cong 1.0$ for large $\bar{E}_1/\bar{E}_2(>10)$, which is also confirmed by our FEM and several other studies (Xia et al. 1993; Suiker and Fleck 2004). Equation 8) is also similar to the so-called *in-situ* strength criterion for transverse cracking in laminated PMCs recently developed by Davila et al.(Davila et al. 2005; Camanho et al. 2006). Unlike traditional strength-based criteria such as the Hashin and Tsai-Wu criteria, this criterion accounts for the effects of ply thickness and the constraint of neighboring plies on the strength of the transverse ply, which are especially important when h is small. As can be seen from Eq. (8), the tunneling stress is inversely proportional to the ply thickness, h, which has been observed by several experimental measurements, e.g. (Wang and Crossman 1982; Wang 1984).

However, while a single scalar criterion for the occurrence of transverse ply cracking such as that of Eq. (8) may be useful for modeling composite damage evolution at length scales greater than the ply thickness, it inevitably possesses shortcomings. One clear shortcoming is its neglect of edge effects such as those seen in Fig. 6. In laminated composites, free edge damage initiation is very common and neither the LEFM-based nor the traditional strength-based criteria address it effectively (Yang 2002; Yang and Cox 2005). The nonlinear cohesive zone models reveal how the free edge is prone to initiation: even if an initial flaw is located in the interior of a laminate, damage or partial damage will quickly tunnel to the free edge. From that point, further damage evolution favors the free edge because the difference in Poisson's ratios between neighboring plies provides additional energy release and creates mode ratios favorable to fracture (mixed mode II and III). Thus even in the delamination-with-tunneling case, Fig. 6(a), upon further loading after completion of the tunneling process, the delamination propagates faster near the free edge than in the interior. In the case of Fig. 6(b) where the coupling mode is tunneling-with-delamination, the coupled tunneling and delamination process always initiates from the free edge and propagates into the specimen interior.

As well as free edge effects, the nonlinear coupling of transverse ply and delamination cracks that is exemplified here can have profound effects on the evolution of damage in other specimen configurations. One example reported elsewhere (Ling et al. 2010) is delamination ply jumping, i.e., the phenomenon of a delamination that jumps from one ply interface to another, which is key to determining damage patterns in composites subjected to complex loads. This process exhibits multi-crack features that can only be predicted by a nonlinear fracture model that treats the infra-ply failure sequence in detail. It cannot be summarized in a single criterion.

5 Conclusions

In this study, the coupled evolution of a transverse intra-ply crack and possible accompanying delamination cracks in a [0/90/0] laminate has been investigated using 3D cohesive elements to represent the nonlinear fracture of both types of crack. A steady-state LEFM solution to the same problem was also derived for comparison.

Nonlinear fracture analysis shows that, for common PMCs, which typically have an interface fracture toughness (approximately Γ_{II}, the mode II toughness) larger than the transverse tunneling fracture toughness (approximately Γ_{I}, the mode I toughness), the delamination process will not develop until the tunneling phase of the transverse crack growth is complete (tunneling-without-delamination mode). The predicted tunneling crack initiation from an arbitrary induced small flaw as a penny-shape crack agrees with the depiction originally presented by Suo and colleagues. However, nonlinearity in the fracture process modifies the subsequent evolution of the crack system towards a mature transverse crack. Phases of the evolution include a second initiation event at the free edge of the specimen, linking of the two initiation events via a tunneling mode, subsequent spreading of the resulting transverse crack through the thickness of the ply, delamination initiation at the interfaces, beginning at the free edge, and finally the opening of the transverse crack until it is completely stress-free.

Although the tunneling process is slightly different from the steady-state tunneling assumption in prior LEFM analyses, for toughness ratios $\Gamma_{\mathrm{II}}/\Gamma_{\mathrm{I}}$ representative of PMCs, the nonlinear fracture model predicts a tunneling stress close to the LEFM prediction. In contrast, for similar material parameters, LEFM cannot predict delamination initiation or early growth, becoming accurate only when the delamination crack length ($2l$) is larger than twice the ply thickness ($2h$). The delamination initiation stress depends on toughness ratio as well as on cohesive strength.

The tunneling-without-delamination mode is numerically stable except in the delamination initiation phase, where instability occurs at small delamination crack lengths ($l/h < 1$); but stability returns when the delamination crack length increases to $l/h > 2$. Numerical difficulty associated with this instability can be circumvented by increasing the equilibrium iteration number (in ABAQUS) to allow for failure of many CZM elements simultaneously along the crack path until the stability is regained due to increased delamination length ($l/h > 1$).

When the toughness ratio Γ_{II}/Γ_I is small (0.1–0.5), the unstable tunneling-with-delamination mode occurs. In such cases, the tunneling crack always initiates from the stress-free edge and propagates into the laminate, accompanied by unstable triangular delamination cracks. Direct dynamic simulation based on an explicit formulation is needed to resolve the unstable delamination process.

Acknowledgments Work is supported by NASA Langley Research Center (Contract No. NNL08AA19C).

References

Belytschko T, Black T (1999) Elastic crack growth in finite elements with minimal remeshing. Int J Numer Methods Eng 45:601–620

Borg R, Nilsson L et al (2004) Simulating DCB, ENF, and MMB experiments using shell elements and a cohesive zone model. Composites Sci Technol 64:269–278

Camanho PP, Davila CG et al (2003) Numerical simulation of mixed-mode progressive delamination in composite materials. J Composite Mater 37:1415–1438

Camanho PP, Davila CG et al (2006) Prediction of in situ strengths and matrix cracking in composites under transverse tension and in-plane shear. Composite Part A: Appl Sci Manufacturing 37:165–176

Case SW, Reifsnider KL (1999) MRLife 12 theory manual—composite materials. Materials Response Group, Virginia Polytechnical Institute and State University

Cavalli MN, Thouless MD (2001) The effect of damage nucleation on the toughness of an adhesive joint. J Adhesion 76:75–92

Chang KY, Liu S et al (1991) Damage tolerance of laminated composites containing an open hole and subjected to tensile loadings. J Composite Mater 25:274–301

Cottrell AH (1963) Mechanics of fracture. Tewksbury symposium on fracture, University of Melbourne, Melbourne, Australia

Cox BN, Marshall DB (1996) Crack initiation in fiber-reinforced brittle laminates. J Am Ceram Soc 79:1181–1188

Cox BN, Yang QD (2006) In quest of virtual tests for structural composites. Science 314:1102–1107

Davila CG, Camanho PP et al (2005) Failure criteria for FPR laminates. J Composite Mater 39:323–345

Dollar A, Steif PS (1991) The branched crack problem revisited. J Appl Mech 58:584–586

Geers MGD (1999) Enhanced solution control for physically and geometrically nonlinear problems. Part II—comparative performance analysis. Int J Numer Methods Eng 46: 205–230

Gonzalez C, LLorca J (2006) Multiscale modeling of fracture in fiber-reinforced composites. Acta Materialia 54:4171–4181

Hallett S, Wisnom MR (2006) Numerical investigation of progressive damage and the effect of layup in notched tensile tests. J Composites Mater 40:1229–1245

Hansbo A, Hansbo P (2004) A finite element method for the simulation of strong and weak discontinuities in solid mechanics. Comput Methods Appl Mech Eng 193:3523–3540

He M-Y, Hutchinson JW (1989) Crack deflection at an interface between dissimilar materials. Int J Solids Struct 25:1053–1067

Hillerborg A, Modeer M et al (1976) Analysis of crack formation and crack growth in concrete by means of fracture mechanics and finite elements. Cement Concrete Res 6:773–782

Ho S, Suo Z (1993) Tunneling cracks in constraint layers. ASME J Appl Mech 60:890–894

Hoiseth K, Qu J (2003) Cracking paths at the ply interface in a cross-ply laminate. Composites Part B 34:437–445

Hutchinson JW, Suo Z (1992) Mixed mode cracking in layered materials. Adv Appl Mech 29:63–191

Iarve EV, Mollenhauer D et al (2005) Theoretical and experimental investigation of stress redistribution in open-hole composite laminates due to damage accumulation. Composites: Part A 36:163–171

Ling DS, Fang XJ et al (2010) Nonlinear fracture analysis of delamination crack jumps in laminated composites. J Aerospace Eng (in press)

Ling DS, Yang QD et al (2009) An augmented finite element method for modeling arbitrary discontinuities in composite materials. Inter J Fract 156:53–73

Lu T-J (1996) Crack branching in all-oxide composites. J Am Ceram Soc 79(1):266–274

Massabò R, Cox BN (1999) Concepts for bridged mode II delamination cracks. J Mech Phys Solids 47:1265–1300

McCartney LN (2003) Physically based damage models for laminated composites. J Mater: Design Appl 217(3):163–199

Mergheim J, Kuhl E et al (2005) A finite element method for the computational modeling of cohesive cracks. Int J Numerical Methods Eng 63:276–289

Mergheim J, Kuhl E et al (2007) Towards the algorithmic treatment of 3D strong discontinuities. Commun Numer Methods Eng 23:97–108

Moes N, Belytschko T (2002) Extended finite element method for cohesive crack growth. Eng Fracture Mech 69:813–833

Parmigiani J, Thouless MD (2006) The roles of toughness and cohesive strength on crack deflection at interfaces. J Mech Phys Solids 54:266–287

Rice JR (1980) The mechanics of earthquake rupture. In: Dziewonski AM, Boschi E (eds) Proceedings of the International School of Physics "Enrico Fermi", Course 781979,

Physics of the Earth's Interior, Italian Physical Society and North-Holland Publ Co, pp 555–649

Shahwan KW, Waas AM (1997) Non-self-similar decohesion along a finite interface of unilaterally constrained delaminations. Proc Royal Soc London A 453:515–550

Song SJ, Waas AM (1994) Energy-based mechanical model for mixed mode failure of laminated composites. J Eng Mater Technol 116:512–516

Spearing SM, Beaumont PWR (1992) Fatigue amage mechanics of composite materials. I: experimental measurement of damage and post-fatigue properties. Composites Sci Technol 44:159–168

Suiker ASJ, Fleck NA (2004) Crack tunneling and plane strain delamination in layered solids. Int J Fracture 125:1–32

Talreja R (2006) Mulitscale modeling in damage mechanics of composite materials. J Mater Sci 41:6800–6812

Tay T-E (2003) Characterization and analysis of delamination fracture in composites: an overview of developments from 1990 to 2001. Appl Mech Rev 56(1):1–32

Thouless MD, Yang QD (2001) Measurement and analysis of the fracture properties of adhesive joints. In Dillard DA, Pocious AV, Chaudhury M (eds) The Mechanics of adhesion, vol 1. Elsevier Science, Amsterdam, The Netherlands, pp 235–271

Turon A, Camanho PP et al (2005) A damage model for the simulation of delamination in advanced composites under variable-mode loading. Mech Mater 38:1072–1089

Tvergaard V, Hutchinson JW (1993) The influence of plasticity on the mixed-mode interface toughness. J Mech Phys Solids 41:1119–1135

Van de Meer FP, Sluys LJ (2008) Continuum models for the analysis of progressive failure in composite laminates. J Composite Mater (in press)

Verhoosel CV, Remmers JJC, Gutierrez MA (2008) A dissipation-based arc-length method for robust simulation of brittle and ductile failure. Int J Numer Methods Eng 77:1290–1321

Wang ASD (1984) Fracture mechanics of sublaminate cracks in composite materials. Composite Technol Rev 6:45–62

Wang ASD, Crossman FW (1982) Fracture mechanics of transverse cracks and edge delamination in graphite-epoxy composite laminates. AFOSR Report: 167p.

Wang JS, Suo Z (1990) Experimental determination of interfacial toughness using Brazil-nut-sandwich. Acta Metallurgica 38:1279–1290

Xia ZC, Carr RR et al (1993) Transverse cracking in fiber-reinforced brittle matrix, cross-ply laminates. Acta Met Mater 41(8):2365–2376

Xia ZC, Hutchinson JW (1994) Matrix cracking of cross-ply ceramic composites. Acta Met Mater 42(6):1933–1945

Yang B (2002) Examination of free edge crack nucleation of around an open hole in composite laminates. Int J Fracture 115:173–191

Yang QD, Cox BN (2005) Cohesive models for damage evolution in laminated composites. Int J Fracture 133(2): 107–137

Yang QD, Cox BN et al (2006) Fracture and length scales in human cortical bone: the necessity of Nonlinear Fracture Models. Biomaterials 27:2095–2113

Yang QD, Fang XJ, Shi JX, Lua J (2010) An improved cohesive element for shell delamnation analysis. Int J Numer Methods Eng (in press)

Yang QD, Thouless MD (2001) Mixed mode fracture of plastically-deforming adhesive joints. Int J Fracture 110: 175–187

Ye T, Suo Z et al (1992) Thin film cracking and the roles of substrate and interface. Int J Solids Struct 29:2639–2648

Zhang Y, Wang S (2009) Buckling, post-buckling and delamination propagation in debonded composite laminates. Part I: Theoretical development. Composite Struct 88: 121–130